Investigating Molecular Exciton-Polaritons using Many-body Electronic Structure Theory with Cavity Quantum Electrodynamics

Braden M. Weight,*,† Todd D. Krauss,‡,¶ and Pengfei Huo*,‡,¶

†*Department of Physics and Astronomy, University of Rochester, Rochester, NY 14627, U.S.A.*
‡*Department of Chemistry, University of Rochester, Rochester, NY 14627, U.S.A.*
¶*The Institute of Optics, Hajim School of Engineering, University of Rochester, Rochester, NY 14627, U.S.A.*

E-mail: bweight@ur.rochester.edu; pengfei.huo@rochester.edu

Abstract

Polariton chemistry has emerged recently as a new way to control chemistry using the quantum light-matter interactions by coupling molecules with an optical cavity. Much of the recent theoretical work in understanding exciton-polaritons has stemmed from reformulating electronic structure software to include the interactions between photonic and molecular degrees of freedom. In this work, we present a conceptually simple framework to uncovering these phenomena utilizing already-made and heavily tested electronic structure packages for the complicated molecular Hamiltonian and simply combining this information into the popular Pauli-Fierz Hamiltonian to perform a second diagonalization to obtain the polaritonic properties. In this way, we can also easily compute various quantities useful for analysis of the polaritonic excited states, including the transition density matrix, real-space projected transition density, mixed electron-photon transition density, natural transition orbitals, and linear spectroscopy.

Introduction. Coupling molecules to the quantized radiation field inside an optical cavity creates a set of new photon-matter hybrid states, so-called polariton states.[1–3] These polariton states have delocalized excitations among molecules and the cavity mode, which have been shown to facilitate new chemical reactivities.[1,3,4] Theoretical investigations play a crucial role in understanding new principles in this emerging field and have suggested interesting reaction mechanisms enabled by cavity Quantum Electrodynamics (QED).[5–14] Polariton chemistry thus provides a new strategy to control chemical reactivity in a general way by tuning the fundamental properties of photons and provides a new paradigm for enabling chemical transformations that can profoundly impact catalysis, energy production, and the field of chemistry at large.

Theoretical investigations play a crucial role in understanding new principles in this emerging field and have suggested interesting reaction mechanisms enabled by cavity quantum electrodynamics (QED).[9,14–36] In recent works, traditional electronic structure methods have been generalized to include the effects of light-matter interactions and used to solve the polaritonic states of the molecule-cavity hybrid systems. To name a few, these efforts include the cavity QED density functional theory (QED-DFT),[29,32,37,38] time-dependent DFT (QED-TD-DFT),[29,31,39–41] coupled cluster (QED-CC) and its equation-of-motion extension (QED-EOM-CC),[33,33,37,42] or full configuration interaction (FCI) methods.[37,43] In this way, the light and matter description are calculated on the same footing in their respective methodologies, where the to-

tal polariton wavefunction is expressed as the linear combination of different configurations (*e.g.*, Slater determinants of single-particle states), with each configuration composed as a tensor product of the electronic configuration and the photonic configuration. In this work, these schemes will be denoted as self-consistent quantum electrodynamical (scQED) methods.

An alternative approach is to solve the same problem in two steps. This procedure involves obtaining the electronic adiabatic states (eigenstates of the adiabatic molecular Hamiltonian, see Eq. 2) using any of the previously mentioned traditional electronic structure methods and then constructing the total polariton wavefunction using these adiabatic states for the molecule – and Fock states for the photonic modes – through diagonalization of the total light-matter Hamiltonian. For this procedure, only the molecular energies and dipole operator matrix elements are required as input in the dipole-gauge Pauli-Fierz Hamiltonian (see Eq. 1 in Theoretical and Computational Methods section). In this work, this procedure is referred to as the parameterized QED (pQED) scheme.

In principle, both pQED and scQED will generate identical results under the complete basis limit. Compared to scQED, the pQED scheme is much simpler in the sense that it does not require additional re-development of electronic structure theory for the QED Hamiltonian as well as the simplicity that comes with a non-self-consistent solution. Despite the enormous recent progress in scQED and pQED schemes, what is generally missing is a *consistent comparison* of both approaches and assessment of the strengths/limitations of each method under different scenarios. In particular, an open question in the field of *ab initio* polariton chemistry is whether a pQED calculation can provide the same level of accuracy compared to the scQED simulation.[40,44,45]

In this work, we use the pQED approach to compute polariton properties and directly compare to the existing work based on the scQED approaches. We will directly assess the accuracy of the pQED approach by computing the eigenspectrum of the polaritonic system. Further, we also present new theoretical metrics to analyze the excited state properties of the molecule-cavity hybrid systems, which will be a valuable tool to understand how forming polaritons can influence the excited state properties of the molecule. Finally, we will investigate how forming polaritons can influence the fundamental property of molecules, including dramatically changing the excited state character of the polyphenyl ether (PPE) molecule, as well as compute the polariton eigenspectra and absoprtion spectra of coupling a single-walled carbon nanotube (SWCNT) that contains ∼1000 carbon atoms with an optical cavity.

Theoretical Approach. We use the Pauli-Fierz (PF) Hamiltonian[38,46–48] to describe the interactions between *ab initio* molecular systems and the photon field. The PF Hamiltonian can be written as follows

$$\begin{aligned}\hat{H}_{\rm PF} =& \hat{H}_{\rm M} + \hbar\omega_{\rm c}\big(\hat{a}^\dagger\hat{a} + \frac{1}{2}\big) \\ &+ \omega_{\rm c}\mathbf{A_0}\cdot\hat{\boldsymbol{\mu}}(\hat{a}^\dagger + \hat{a}) + \frac{\omega_{\rm c}}{\hbar}(\mathbf{A_0}\cdot\hat{\boldsymbol{\mu}})^2,\end{aligned} \tag{1}$$

where the $\hat{H}_{\rm M}$ is the bare molecular Hamiltonian, $\hbar\omega_{\rm c}\big(\hat{a}^\dagger\hat{a}+\frac{1}{2}\big)$ is the cavity photon field Hamiltonian (under the single mode assumption), $\omega_{\rm c}\mathbf{A_0}\cdot\hat{\boldsymbol{\mu}}(\hat{a}^\dagger + \hat{a})$ is the molecular-cavity coupling term under the dipole (length) gauge, and $\frac{\omega_{\rm c}}{\hbar}(\mathbf{A_0}\cdot\hat{\mu})^2$ is the dipole self-energy, which is an essential for the correct description of a bounded ground state[46] as well as for including other effects for energy and off-diagonal coupling corrections at large light-matter coupling strengths.

The total dipole operator of the molecule is $\hat{\boldsymbol{\mu}} = \sum_i z_i\hat{\mathbf{R}}_i - \sum_k \hat{\mathbf{r}}_k$, where $\hat{\mathbf{R}}_i$ is the position operator of nucleus i, with charge z_i, and $\hat{\mathbf{r}}_k$ is the position operator of electron k (with the unit negative charge). Further, $\omega_{\rm c}$ is the frequency of the mode in the cavity, $\hat{a}^\dagger$ and $\hat{a}$ are the photonic creation and annihilation operators, and $\hat{q}_{\rm c} = \sqrt{\hbar/2\omega_{\rm c}}(\hat{a}^\dagger + \hat{a})$ and $\hat{p}_{\rm c} = i\sqrt{\hbar\omega_{\rm c}/2}(\hat{a}^\dagger - \hat{a})$ are the photonic coordinate and momentum operators, respectively. For a FP cavity, the coupling strength is $\mathbf{A}_0 = A_0\hat{\mathbf{e}}$, where $\hat{\mathbf{e}}$ is the unit vector of the field polarization and $A_0 = \sqrt{\hbar/2\omega_{\rm c}\varepsilon_0\mathcal{V}}$ is the field intensity, $\mathcal{V}$ is the quantization volume inside the cavity, ε_0 is the permittivity. Throughout this letter, we treat A_0 (in atomic units) as a parameter. This parameter is related to the commonly used Jaynes-Cummings (JC) Hamiltonian coupling strength $g_{\rm c}$ where $g_{\rm c} = \omega_{\rm c}A_0\mu_{01}$ for a two-level electronic system transition dipole μ_{01}. As a concrete example, if $\omega_c = 5.0$ eV, $A_0 = 0.01$ a.u., and $\mu_{01} = 5.0$ a.u. – which will be average parameters in this letter, then $g_c \approx 0.01$ a.u. with a Rabi frequency of $\Omega_R = 2g_c = 0.04$ a.u. Although, it should be noted that including a many-level generalization, including DSE and highly oscillatory terms (*i.e.*,

not making the rotating wave approximation) as is done in the full PF Hamiltonian causes this direct analogy to be weak as more complex effects arise at large coupling strengths where non-linear effects are ubiquitous.

The molecular Hamiltonian (in the position representation) is expressed as $\hat{H}_{\rm M} = \hat{\mathbf{T}}_{\mathbf{R}} + \hat{H}_{\rm el}(\mathbf{r}, \mathbf{R})$, where $\hat{\mathbf{T}}_{\mathbf{R}} = -\sum_i \hbar^2 \nabla^2_{\mathbf{R}_i}/2M_i$ is the nuclear kinetic energy operator, $\hat{H}_{\rm el}(\mathbf{r}, \mathbf{R}) = \hat{\mathbf{T}}_{\mathbf{r}} + \hat{V}_{\rm coul}(\mathbf{r}, \mathbf{R})$ is the electronic Hamiltonian, with the electronic kinetic energy $\hat{\mathbf{T}}_{\mathbf{r}}$ and Coulomb potential $\hat{V}_{\rm coul}(\mathbf{R}, \mathbf{r})$ among electrons and nuclei. The electronic adiabatic state $|\psi_\alpha(\mathbf{R})\rangle$ is defined as the eigenstate of $\hat{H}_{\rm el}$ as,

$$\hat{H}_{\rm el}|\psi_\alpha(\mathbf{R})\rangle = E_\alpha(\mathbf{R})|\psi_\alpha(\mathbf{R})\rangle, \tag{2}$$

where $\alpha = 0, 1, 2...$, and $|\psi_0(\mathbf{R})\rangle$ is the ground electronic state of the matter. The matrix elements of the total dipole operators can be obtained using the adiabatic states as,

$$\mu_{\alpha\beta}(\mathbf{R}) = \langle\psi_\alpha(\mathbf{R})|\hat{\mu}|\psi_\beta(\mathbf{R})\rangle. \tag{3}$$

In a similar sense of defining the electronic Hamiltonian and corresponding eigenvalue equation for the matter, one can define a similar expression for the polaritonic system,[31,38,40,44,49] $\hat{H}_{\rm pl} \equiv \hat{H}_{\rm PF} - \hat{\mathbf{T}}_R$, which includes all operators of molecules and cavity, except for the nuclear kinetic energy operator $\hat{\mathbf{T}}_R$. As such, the polariton state is defined as the eigenstate of $\hat{H}_{\rm pl}$ through the following eigenvalue problem

$$(\hat{H}_{\rm PF} - \hat{\mathbf{T}}_{\mathbf{R}})|\Phi_j(\mathbf{R})\rangle = \mathcal{E}_j(\mathbf{R})|\Phi_j(\mathbf{R})\rangle, \tag{4}$$

where $\hat{H}_{\rm pl} \equiv \hat{H}_{\rm PF} - \hat{\mathbf{T}}_R$ is the polariton Hamiltonian, $|\Phi_j(\mathbf{R})\rangle$ is the polariton eigenstate, and $\mathcal{E}_j(\mathbf{R})$ is the polariton potential energy surface. As can be seen clearly, both $|\Phi_j(\mathbf{R})\rangle$ and $\mathcal{E}_j(\mathbf{R})$ parametrically depends on the nuclear configuration $\mathbf{R}$. We denote $|\Phi_0\rangle$ as the ground state of polariton Hamiltonian.

To solve the eigenvalue problem in Eq. 4, one can represent the polaritonic state through the convenient adiabatic-Fock basis as,

$$|\Phi_j(\mathbf{R})\rangle = \sum_{\alpha,n} C^j_{\alpha n}|\psi_\alpha(\mathbf{R})\rangle \otimes |n\rangle, \tag{5}$$

where $C^j_{\alpha n}$ is the expansion coefficient of the $j_{\rm th}$ polariton for the $\alpha n_{\rm th}$ basis state, $|\psi_\alpha(\mathbf{R})\rangle$ is the $\alpha_{\rm th}$ electronic adiabatic state (*i.e.*, the eigenstate of $\hat{H}_{\rm el}$ in Eq. 2), and $|n\rangle$ is the Fock/number state (*i.e.*, the eigenstate of $\hbar\omega_{\rm c}(\hat{a}^\dagger\hat{a} + \frac{1}{2})$). At a particular molecular geometry, direct diagonalization of the polaritonic matrix, with matrix elements defined as $\langle\psi_\beta, m|\hat{H}_{\rm pl}|\psi_\alpha, n\rangle$, provides both expansion coefficients $C^j_{\alpha n} = \langle\psi_\alpha(\mathbf{R}), n|\Phi_j(\mathbf{R})\rangle$, as well as the polariton eigenenergy $\mathcal{E}_j(\mathbf{R})$.

All polaritonic observables in this letter between the ground and the $j_{\rm th}$ polariton state are conveniently computed as

$$\begin{aligned}(\hat{A}\hat{B})_{0j} &= \langle\Phi_0(\mathbf{R})|\hat{A}_{\rm el} \otimes \hat{B}_{\rm ph}|\Phi_j(\mathbf{R})\rangle \\ &= \sum_{\alpha n}\sum_{\beta m} C^0_{\alpha n} C^j_{\beta m}\langle\psi_\alpha(\mathbf{R})|\hat{A}_{\rm el}|\psi_\beta(\mathbf{R})\rangle \otimes \langle n|\hat{B}_{\rm ph}|m\rangle,\end{aligned} \tag{6}$$

where $\hat{A}_{\rm el}$ and $\hat{B}_{\rm ph}$ are operators in the electronic and photonic Hilbert sub-spaces, respectively, $\{|\psi_\alpha(\mathbf{R})\rangle, |\psi_\beta(\mathbf{R})\rangle\}$ are electronic adiabatic states, $\{|n\rangle, |m\rangle\}$ are photonic Fock/number states, and $\{C^j_{\alpha,n}\}$ is are the expansion coefficients in Eq. 5 in the adiabtic-Fock basis. For example, $A_{\alpha\beta}$ may be the molecular dipole matrix, transition density, or natural transition orbitals, while B_{nm} may be the photon number matrix, photonic transition density, or photonic dipole matrix. See **Theoretical Details** for more information on the computation of the individual electronic and photonic properties.

With this approach, one must *necessarily* treat the number of electronic and photonic basis states as convergence parameters for the polaritonic properties (*e.g.*, the energy $\mathcal{E}_j(\mathbf{R})$) (Fig. S1).[40] For practical use, one can further truncate the electronic basis to a more reasonable number while obtaining identical chemical insight with the dominating error stemming from the choice of electronic structure method (as shown in Table **??**).

This provides a convenient and straightforward approach, due to the extensive, thoroughly tested, and commercially available methods developed in the electronic structure community to solve Eq. 2 in an accurate and efficient fashion. This approach does not require any redevelopment of new electronic-photonic structure theory but rather utilizing what is already available for a new purpose. More details of using this approach to compute the excited state properties are described in the **Theoretical Details** together with brief computational details at the end of this letter as well as in the Supporting Information.

First, we consider the ground state energy of the coupled molecule-cavity hybrid system. Fig. 1

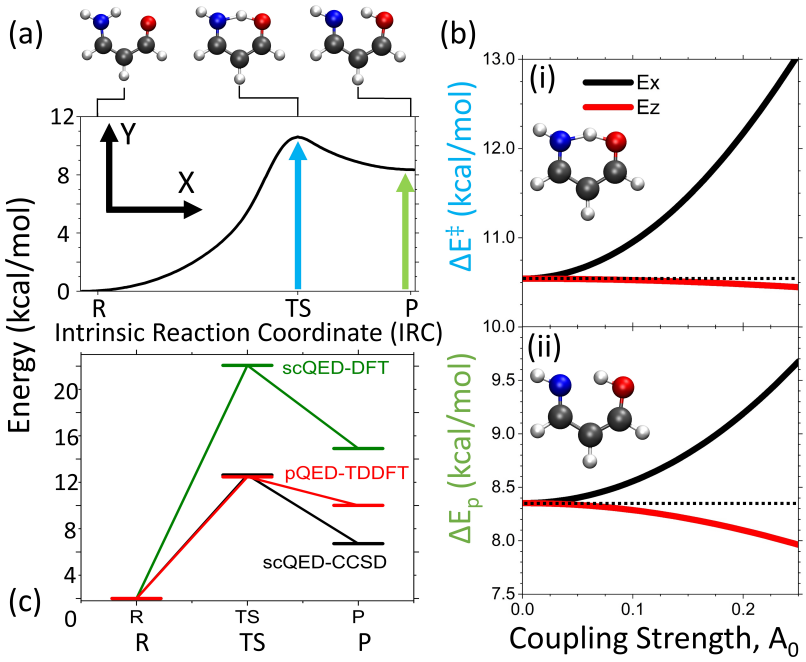

Figure 1: (a) Potential energy surface (PES) as computed from the intrinsic reaction coordinate (IRC) method for the aminopropenal proton transfer reaction showing an asymmetric PES with barrier height $\sim$ 10.5 kcal/mol and thermodynamic potential (product energy) of $\sim$ 8.5 kcal/mol. (b) Energy of the (i) barrier (TS) and (ii) product (P) species as functions of the coupling strength A_0 inside a cavity of frequency $\omega_c = 3.0$ eV with cavity polarizations in both the X- (solid, black line) and Z- (solid, red line) directions. (c) Energy relative to the reactant for the transition state and product species with an X-polarized cavity using scQED-DFT/OEP [50] (green), scQED-CCSD [50] (black) and pQED-TD-DFT/ωB97XD (red).

presents a cavity mediated proton-transfer reaction by coupling the aminopropenal molecule to the cavity. This system was recently reported in Ref. 50 utilizing the modified electronic structure methods scQED-HF, scQED-DFT, and scQED-CC to examine the ground state barrier and product energies of the proton reaction. This asymmetric reaction is thus a perfect example to assess the accuracy of the corresponding pQED calculations

Fig. 1a presents the potential energy surface (PES) of the reaction outside the cavity, computed using the intrinsic reaction coordinate (IRC) method at the density functional theory (DFT) level (see Theoretical and Computational Methods section). The reaction has a large potential energy barrier around 10 kcal/mol from the reactant (R) to the transition state (TS). This is in nearly perfect agreement with the CC results from Ref. 50. However, the energy difference between the reactant and product from the DFT calculation ($\sim$ 8 kcal/mol) is much larger than the CC results (5 kcal/mol), due to the limitations of DFT. Following the previous work,[50] we define the X- and Y-direction of the molecule, indicated in the inset of Fig. 1a. The Z-direction is perpendicular to the defined X-Y plane. We will place the cavity polarization direction $\hat{\mathbf{e}}$ will be aligned with either X- or Z-direction of the molecule. Coupling this molecule to an optical cavity can have a strong influence on the PES, depending on the polarization of the cavity with respect to the molecular orientation.

Fig. 1b(i) presents the TS barrier height $\Delta E^{\ddagger} = \mathcal{E}_0(\mathbf{R}_{\rm TS}) - \mathcal{E}_0(\mathbf{R}_{\rm Reac})$ (polariton energy difference between transition state and reactant nuclear configuration) on the polariton ground state $|\Phi_0(\mathbf{R})\rangle$ as a function of the light-matter coupling A_0 a.u. with the cavity frequency set to $\omega_{\rm c} = 3.0$ eV. The optimized reactant, transition state (TS), and product geometries were calculated outside the cavity, as was done in Ref. 50, which will be used for direct comparison. Note that the mechanism for modifying the group state potential energy surface in this case due to the coupling to the excited states, which is different than the recent studies of vibrational strong coupling.[15] The X-polarization (solid black line) demonstrates a larger effects on barrier height, because there exists a strong transition dipole between the ground state and second electronic excited state ($\mu^x_{01} \sim 1.47/1.26$ a.u.) as well as strong ground state permanent dipole

($\mu_{00}^{x} \sim 1.37/0.90$ a.u.) in the reactant/transition-state geometries (see Fig. S2 in the Supporting Information for dipole matrices for aminopropenal at the reactant, transition state, and product geometries, including the 20 lowest-energy adiabtic states). The magnitude of the ground-to-excited transition dipole in the Z-direction is almost negligible in comparison showing only a slight decrease in the barrier height (solid, red line).

Fig. 1b(ii) examines the effects on the product energy $\Delta E_{\rm p} = \mathcal{E}_0(\mathbf{R}_{\rm Prod}) - \mathcal{E}_0(\mathbf{R}_{\rm Reac})$ on the polariton ground state $|\Phi_0(\mathbf{R})\rangle$ as a function of coupling strength A_0 with the same cavity frequency of $\omega_c = 3.0$ eV. The effects of the cavity for the product energy are reduced for the X-polarization, in comparison to the TS, while increased for the Z-polarization. Similarly to the TS geometry, the X-polarization presents a continuous increase to the energy while the Z-polarization shows a slight decrease. The influence of the Z-polarized cavity on $\Delta E^{\ddagger}$ (panel b(i)) and $\Delta E_{\rm p}$ (panel b(ii)) obtained from the pQED-TD-DFT calculation is also consistent with the previous work[50] using the scQED-CC approach. In particular, with the Z-polarization and a coupling strength of $A_0 = 0.22$ a.u., the difference between the prediction of $\Delta E^{\ddagger}$ obtained from the pQED-TD-DFT and scQED-CC methods is less than 10 meV. For $\Delta E_{\rm p}$, the difference between the two methods is less than 5 meV. This further exemplifies that the pQED-TD-DFT method and the scQED-CC methods provide the same quantitative description for the prediction of $\Delta E_{\rm p}$ and $\Delta E^{\ddagger}$, without the additional effort of developing new DFT functionals. That said, the accuracy of the electronic structure method (which provide the electronic energy and transition dipole moments, see Fig. S2) do play an important role role for providing accurate polariton eigenstates.

For a direct comparison to self-consistent methods, Fig. 1c showcases the scQED-DFT/OEP,[50] scQED-CCSD,[50] and pQED-TD-DFT/ωB97XD methods in calculating the transition state (TS) and product (P) ground state reaction points. We will assume scQED-CCSD to achieve a superior accuracy to either of the two additional methods presented and is taken as the benchmark. The scQED-DFT/OEP method showcases much higher barrier and product energies relative to the reactant, by roughly $\sim$8 kcal/mol in comparison to the scQED-CCSD result. The pQED-TD-DFT/ωB97XD results showcases near-perfect agreement with the scQED-CCSD transition state while exhibiting an overetimation of the product energy by $\sim$4 kcal/mol. It should be noted that the level of DFT used in this work was at the hybrid ωB97XD level while in Ref. 50, a new functional was used that includes approximate electron and photonic exchange-correlation referred to as the optimized-effective potential (OEP) approximation.[32] The differences in the cavity effects between the scQED-CCSD and the method used in this work are less than 30 meV, which is well-within the degree of accuracy between DFT and CC levels of theory for these systems. As expected, the physics of the system is well-represented using either pQED and scQED methods and the overall accuracy is dictated by the choice of underlying electronic structure theory used as input.

Fig. 2 presents the results of molecular polaritons generated by coupling the excited electronic states of the formaldehyde molecule with a single-mode cavity for various cavity frequencies $\omega_{\rm c}$ and coupling strength A_0. We chose this system and parameters based on the recent theoretical simulations in Ref. 31 using the scQED-TD-DFT scheme. Here, we use the pQED-TD-DFT procedure to obtain the polariton PES and transition density (see **Theoretical Details**) for the coupled molecule-cavity hybrid systems. Fig. 2a presents the two lowest-energy ^{1}A$_1$-symmetry excited states of the formaldehyde molecule as a function of the C-O bond length, which are denoted as $|\psi_1^{\rm A_1}\rangle$ and $|\psi_2^{\rm A_1}\rangle$. They are the adiabatic states of $\hat{H}_{\rm el}$. The C-O bond length was scanned by changing only the location of the oxygen atom, keeping all other nuclei frozen. At the C-O bond length of 1.22 Å, these two states correspond to $|\psi_4(\mathbf{R})\rangle$ and $|\psi_7(\mathbf{R})\rangle$. At other C-O bond lengths, these two states may correspond to different labels of the adiabatic states due to the presence of other adiabatic states with a different symmetry and trivial crossings with these two states. The symmetry of the adiabtic state determines the orientation of the non-zero transition dipole. Note that there is an avoided crossing near 1.3-1.4 Å of the C-O bond, with a energy gap of roughly 75 meV (see inset) for this level of theory. Fig. 2b,c present the polaritonic PESs $\mathcal{E}_j(\mathbf{R})$ (defined in Eq. 4) for the system in a cavity with the polarization direction $\hat{\mathbf{e}}$ along the C-O bond, and a cavity photon frequency of $\hbar\omega_{\rm c} = 6.5$ eV (Fig. 2b) and $\hbar\omega_{\rm c} = 9.5$ eV (Fig. 2c), respectively. The character of the polaritonic excited state are color coded according to the photon number in the cavity (right).

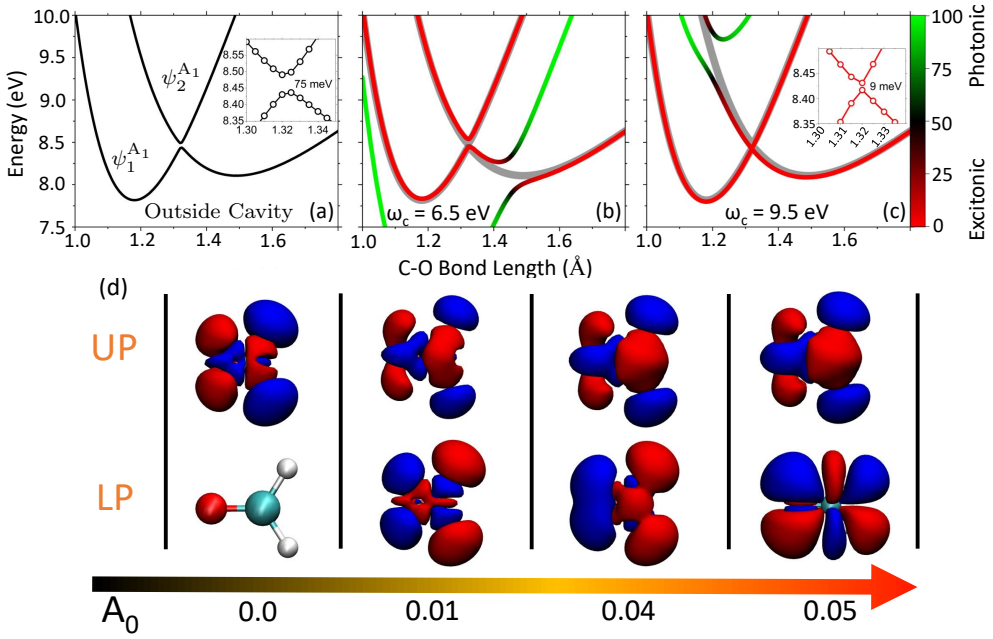

Figure 2: (a) Adiabatic potential energy surface of the formaldehyde molecule's A_1-symmetry excited states as a function of the C-O bond length. The inset presents the avoided crossing between the two adiabatic states. (b)-(c): Polariton excited state energy $\mathcal{E}_j(R_{\rm CO}) - MIN[\mathcal{E}_0(R_{\rm CO})]$ of the formaldehyde-cavity hybrid system with the coupling strength of $A_0 = 0.04$ a.u., for a cavity frequency (b) $\omega_c = 6.5$ eV and (c) $\omega_c = 9.5$ eV. The cavity polarization $\hat{\mathbf{e}}$ is parallel to the C-O bond vector. For panels (b,c) the color map indicates the photonic character, and the cavity-free electronic states are shown as thick gray lines. The inset in panel c shows the reduction of the avoided crossing from 75 to 9 meV. (d) Transition density $\xi(r_e)$ of the upper (UP) and lower (LP) polaritons for $A_0 = 0$ a.u., 0.01 a.u., 0.04 a.u., and 0.05 a.u. at $\omega_c = 7.92$ eV with a C-O bond length of 1.22 Å.

In Fig. 2b, the green-colored curve is largely composed of the photon-dressed ground state $|\psi_0(R)\rangle \otimes |1\rangle \equiv |\psi_0(R), 1\rangle$. Near to a C-O bond length of 1.45 Å, the $|\psi_0(R)\rangle \otimes |1\rangle$ state crosses the $|\psi_1^{A_1}(R)\rangle \otimes |0\rangle$ state, which is an excited state with 0 photons (thick gray curve in Fig. 2b). The light-matter interaction (in Eq. 1) hybridizes the two states and generates the polaritonic states, with the energy splitting generated commonly referred to as the Rabi splitting. At this nuclear configuration, both polariton states contain roughly equal contributions of the excitonic and photonic character (indicated as 50% on the colorbar as black). Further, the molecule-cavity interaction produces hybridized states with mixed ground and excited adiabatic character. The original adiabatic potential energy minima located near the C-O bond length of 1.5 Å for the lower-energy $\psi_1^{A_1}$ state (see panel a) has now been removed (see panel b). The new lowest-energy excited-state polariton now has a totally downward slope toward the same minimum location as the ground polariton state $|\Phi_0(\mathbf{R})\rangle$, with nearly 100% photonic character (green color) in that region.

Fig. 2c presents similar features of the polariton potential with a cavity frequency of $\hbar\omega_c = 9.5$ eV. For this case, the photon dressed state $|\psi_0(\mathbf{R}), 1\rangle$ (green curve) hybridizes with the $|\psi_2^{A_1}, 0\rangle$ (gray) and generate a large Rabi splitting at $R = 1.25$ Å. Interestingly, due to the light-matter interaction, the middle polariton curve (red curve in R=1.35 Å) in this panel has a lower energy compared to the original adiabatic state $|\psi_2^{A_1}, 0\rangle$ (gray). The inset shows that the avoided crossing has been reduced to 9 meV, a reduction by an order of magnitude compare to the original avoided crossing in the bare molecule (Fig. 2a). This is because that the photon-dressed ground state (green) "pushes" down upon the $\psi_2^{A_1}$ state (due to the light-matter coupling), effectively reducing the magnitude of the avoided crossing. In Supporting Information, we also present the magnitude of the avoided crossing as a function of the cavity energy in Fig. S3b.

Fig. 2d presents the real-space projected transition density (Eq. 13), where the photonic DOFs have been traced out, leaving only the electronic contributions mixed through the polaritonic expansion coefficients in the adiabatic matter/Fock basis (see Eq. 5). The theoretical details on computing the polaritonic transition density calculations

are provided at the end of this letter. The light-matter hybridization leads to super-positions between photon dressed electronic states. This results in changes of the transition density as a function of the coupling strength A_0 (varied along the X-axis of panel d) for the upper and lower polaritons, which correspond to the lowest-energy PESs, with a C-O bond length of 1.22 Å and at cavity energy $\omega_c = 7.92$ eV. Under this configuration, the cavity is nearly resonant with the molecular adiabatic transition from the ground state to the $\psi_1^{A_1}$ state at the Frank-Condon point, according to the previous work in Ref. 31. Through mixing of the characters of electronic states, the transition density is modified for each coupling strength. The transition density obtained from the pQED simulation presented in panel d are visually identical to those obtained from scQED in Ref. 31.

After comparing the pQED method with existing sc-QED approaches, we move toward a discussion of computing and manipulating polaritonic properties in the excited state for interesting chemical and physical processes. Fig. 3 showcases one such example where the intention is to compute various excited state quantities such as the natural transition orbitals (NTOs), transition density matrix, and transition density, which are commonly utilized in the electronic structure community to interpret excitations in molecular systems. See **Theoretical Details** for more information on the computation of these quantities. In particular, we aim to showcase how one is able to *manipulate the character and energetic alignment of an exited charge transfer state* (which is optically inactive) via coupling a nearby excited state with non-zero oscillator strength to the cavity.

The excitations in the bare molecular system are characterized in Fig. 3a via the molecular transition dipole matrix, truncated to the lowest six electronic states. Along the diagonal (permanent dipole elements), the character of each transition is labeled, where R (L) indicates a $\pi\pi^*$ excitation localized on the long right (short left) arm, and CT indicates a charge transfer state between arms. The NTOs outside the cavity are shown in Fig. S4 for the lowest six molecular excitations. In many photovoltaic or light emission applications, one aims to control the energetic positioning of the charge transfer states with respect to other types of excitations, *e.g.*, $\pi\pi^*$, in order to provide the most beneficial pathway for the excited state population. Here, we showcase the ability to control the energetic alignment and character of a low-energy charge transfer state (CT^1) via coupling a higher-energy electronic transition (L) with non-zero oscillator strength to the cavity.

Fig. 3b showcases the polaritonic energy as a function of the coupling strength A_0, where the colorbar indicates the percent of photonic character. Here, the cavity frequency is in resonance with the fifth molecular excitation (L) at $\omega_c = 3.45$ eV with cavity polarization in the X-direction (see inset between panels d and e). Further, Fig. 3c shows the excitonic absorption spectra as a function of coupling strength A_0 (see Theoretical Details), where the vertical dotted lines indicate the cavity frequency (right) and the low-energy ψ_1 transition. Above Fig. 3c, the absorption spectrum outside the cavity is shown. To analyze the character of the low-energy CT^1 excitation as a function of the coupling strength A_0, we compute the (Fig. 3d-f) polaritonic NTOs $(\zeta_d^{H/L})_{\alpha\beta}^{M}$ and (Fig. 3g-i) transition density at three coupling strengths $A_0 = 0.0$, 0.02, and 0.05 a.u. (see **Theoretical Details** for more information on NTOs and transition density). At $A_0 = 0.0$ a.u., the character of the CT^1 exciton is evident as the electron and hole NTOs are spatially separated across both arms while the transition density is only present at the corner where the electron/hole NTOs are strongly overlapping.

At low values of coupling strength $A_0 < 0.02$ a.u., there are a series of crossings between polaritonic states that exhibit a variety of splittings on the order of ∼20 meV or less. Although, most ground-to-excited matter states are little-to-no oscillator strength, all states are coupled by the complex transition dipole matrix (Fig. 3a). The absorption spectra showcases multiple peaks at zero coupling, while at larger coupling ($A_0 < 0.05$ a.u.) all oscillator strength becomes focused into the two main bands except for the oscillator strength originating from the eighth electronic state $|\phi_8\rangle$ which does not strongly couple to the cavity in this polarization.

At increased coupling strength $A_0 = 0.02$ a.u., the character of the second polaritonic state (originally CT^1) becomes mixed with the descending-in-energy polaritonic state largely composed of the original ψ_5 exciton (L) which exhibited a $\pi\pi^*$ excitation localized to the left arm. At $A_0 = 0.02$ a.u., the CT^1 state and the descending polaritonic state are fully mixed which localizes the transition density (Fig. 3h) to the left arm. The NTOs (Fig. 3e) show that the hole is largely unperturbed by the nearby polariton due to the shared hole charac-

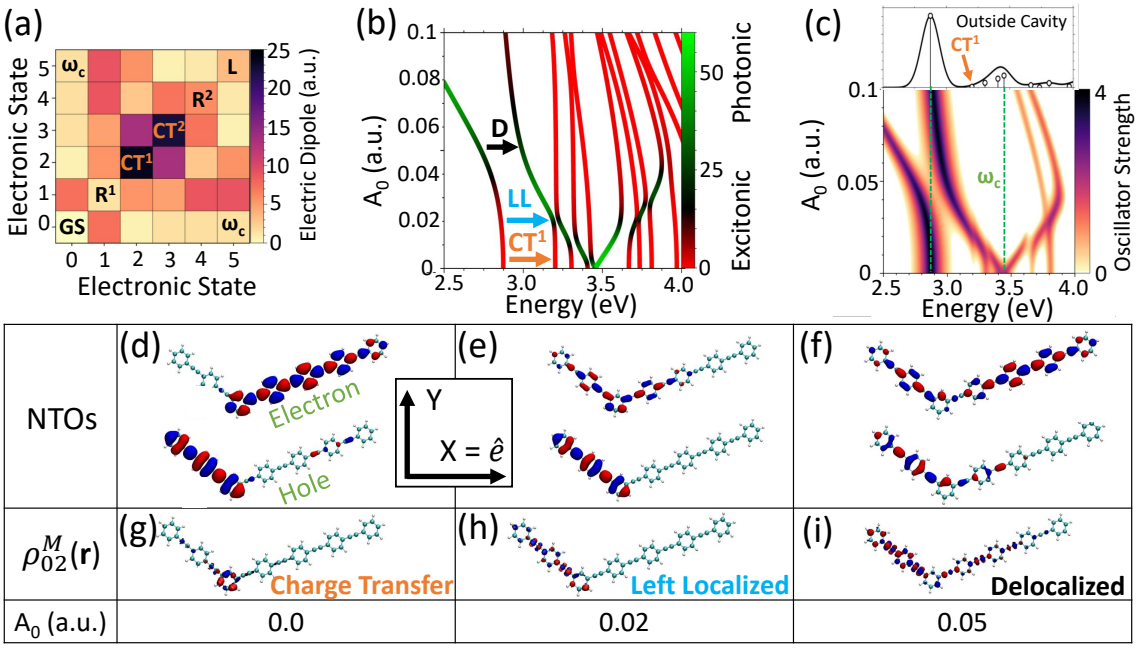

Figure 3: Excited state polariton properties for the 35 PPE molecule coupled to an optical cavity at $\omega_c = 3.45$ eV with cavity polarization in the X-direction (see inset between panels d and 3). (a) Transition dipole matrix of the bare 35PPE molecule (outside the cavity) with labels for the character of each excitation along the permanent dipole of each excited state. In order of increasing energy: ground state (GS), $\pi\pi^*$ transition localized to the right arm (R^1), charge transfer state 1 (CT^1), charge transfer state 2 (CT^2), $\pi\pi^*$ right-localized (R^2), and $\pi\pi^*$ left-localized (L). The color bar indicates the magnitude of the dipole matrix element, and the ω_c label indicates the ground-to-excited bare molecular transition in resonant with the cavity frequency. (b) Polaritonic energy spectrum as a function of coupling strength A_0. The color of the curves denote the percent of photonic character of the state as mostly excitonic (red) or photonic character (green). (c) Excitonic absorption spectra of the 35PPE molecule as a function of the coupling strength A_0. The vertical lines indicate the bare molecular ψ_1 transition energy (left) and the cavity frequency (right) in resonance with the ψ_5 transition energy. See above panel c for the 35PPE absorption spectrum outside the cavity. (d-f) Natural transition orbitals (NTOs) for the ground-to-second polaritonic excitation for three coupling strengths $A_0 = 0.0$, 0.02, and 0.05 a.u. (g-i) Transition density ρ^{M}_{02} for the same coupling strength as (d-f). At zero coupling strength, the second excited polaritonic transition corresponds to the CT^1 state and is tracked by the arrows in panel a for different coupling strengths and labeled by its character in panels (g-i). The isovalue for the transition densities and NTOs were chosen to be 0.001 and 0.02, respectively. The absorption spectra was broadened with a Lorentzian distribution with width $\sigma = 0.1$ eV.

ter between the original CT^1 and the L excitons (see Fig. S4 and Fig. S5 for the transition dipole matrix for the lowest 20 electronic states). The electron distribution is moderately affected moving from completely right-localized to mostly left-localized with some non-zero right-arm character. Additionally, both the hole and electron NTOs are reduced in magnitude due to the non-zero mixture of the cavity photon, which is most prominent for the electron.

At larger coupling ($A_0 = 0.05$ a.u.), the descending polariton interacts with the lowest-energy polaritonic excited state (originally R^1) which then adds right-localized character to the Φ_2 state, effectively delocalizing the transition density across both arms. The NTOs are similarly perturbed showing the electron distribution delocalized while the hole distribution is only weakly delocalized at this coupling strength. As an additional analysis technique, the fragmented polaritonic transition density matrix can be found for both the $|\Phi_1\rangle$ and $|\Phi_2\rangle$ polaritonic excitations in Fig. S6a-c at three values of coupling strength, which gives more information regarding the spatial coherence for each polaritonic excitation.[51] A similar analysis of the modifications to the $|\Phi_1\rangle$ transition can be found in Fig. S6d-f showing that the R^1 state can be similar manipulated to show delocalized character at larger coupling strengths. At this point, the bright character of the R^1 exciton was transferred to the $|\Phi_2\rangle$ state.

In this example, we were able to effectively manipulate the CT^1 state in the bare molecular system by coupling to a higher-energy transition with

non-zero oscillator strength. The character, including the optical activity, of the second polaritonic state was changed to allow experimental tunability of this CT system that can be utilized in realistic light-harvesting or light-emitting systems to achieve a high degree of exciton splitting or radiative recombination, respectively, after photoexcitation processes.

In conclusion of this example, the procedure of utilizing common electronic structure analysis techniques to examine coupled electron-photon systems is largely unchanged and requires little-to-no conceptual extension when one is interested in modifications to the electronic sub-system as a result of the photonic DOFs. Thereby, we propose to utilize the framework already established by the electronic structure community to analyze polaritonic properties of light-matter hybrid systems with the pQED procedure (using Eq. 6 to compute

Fig. S7 in the Supporting Information presents a slightly abstract extension of the real-space transition density matrix (Fig. S6) by now examining the coherence between a single electronic coordinate and a photonic one. The mixed electronic-photonic transition density $\rho_{0j}(r_e, q_c)$ (Eq. S10) for the H_2 molecule is shown for three choices of coupling strengths. Due to the simplicity of the electronic system, the electron and photonic transition densities look very similar and yield conceptually simple results (see Supporting Information for discussion) regarding the mixed coordinate spatial coherence. This analysis tool will have direct application to multi-mode cavities where one is interested in examining the coherence between cavity modes or between electron and photon DOFs for low-frequency cavities where the electron and photon coordinates may, together, provide extremely meaningful insight into the complex interplay between these DOFs.

As our final example, we present results for a single-walled carbon nanotube (SWCNT) system (∼1000 atoms, see **Computational Details**) which has been the subject of recent experimental interest.[52,53] Semi-conducting SWCNTs are known to be ''dark" to emission due to low-lying optically inactive states below the so-called band-edge E_{11} exciton. Fig. 4a provides the transition dipole matrix for the pristine (6,5) SWCNT system, showing a sparse matrix with only the ground-to-E_{11} (*i.e.*, the sixth bare molecular transition) transition to be optically allowed with a large dipole moment of ∼ 28 a.u. with minimal dipole coupling between excited states. This is in strong contrast to previous molecules studied in this work (see Fig. 3a, Fig. S2, Fig. S3, and Fig. S5). The E_{11} transition is just below 2.0 eV, which agrees with previous theoretical calculations of the E_{11} excitonic energy.[54] See above Fig. 4c,d for the real-space projected transition density of the E_{11} ground-to-E_{11} exciton showcasing its delocalized character. Semiconducting SWCNTs, when functionalized with covalent adducts forming a hybridization defect, exhibit bright emission features due to the addition of a defect-associated exciton below the band edge, which have been the subject of much experimental and theoretical work over the last decade for their use as single-photon light sources and for their tunable emission at low-energy telecommunications wavelengths.[54–69] The simplicity of this system's dipole matrix will lead to simple results and a new pathway toward the tunable manipulation of SWCNT without the need for chemical functionalization.

Fig. 4b shows the polaritonic energy as a function of the coupling strength for the SWCNT system when the cavity is in resonance with the bright E_{11} transition, showcasing the many optically inactive (weakly dipole-coupled) molecular states housed in the same region of energy. The colorbar indicates the percent of photonic character. In this case, one is able to note the nearly symmetric Rabi splitting due to the inactivity of the nearby states acting essentially as spectator states until extremely large coupling of $A_0 \sim 0.02$ a.u. where all states begin to exhibit a decrease in energy.

Fig. 4c shows the excitonic spectra of the system inside the cavity (see Theoretical Details) when the cavity energy is at half-resonance with the bright E_{11} transition (i.e., when $|\phi_0, 2\rangle$ is in resonance with $|E_{11}, 0\rangle$) and so shows weak splitting of the effective upper and lower polaritons which form through coupling of the $|\phi_0, 2\rangle$ and $|E_{11} = \phi_6, 0\rangle$ states. At very large coupling strengths, the lowest-energy excited polaritonic state $|\Phi_1\rangle$ becomes partially bright due to the mixing with the E_{11} state over the large energy difference of nearly 1.0 eV. Fig. 4d-f show the same information but with varied cavity energy: (d) 1.5 eV, (e) 2.0 eV, (f) 2.5 eV. Interestingly, the resonant case (panel e) shows nearly perfect Rabi splitting (denoted as Ω_R) as a function of coupling strength. The weakly negative (panel d) and positive (panel f) detunings showcase a very important result. Here, one can demonstrate that the bright character of the

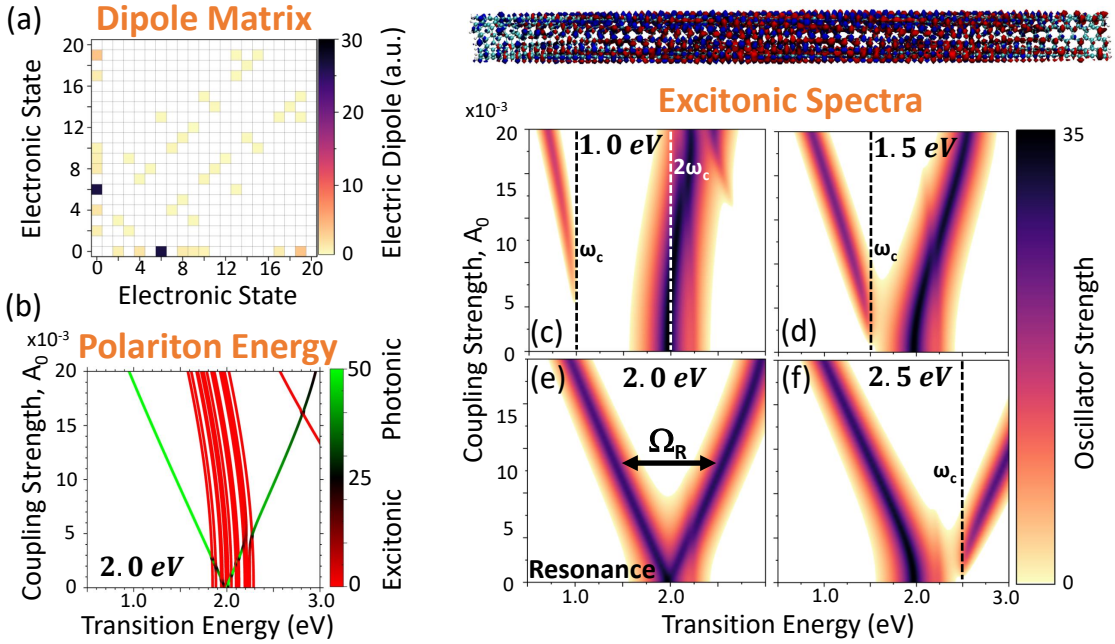

Figure 4: (a) Electronic transition dipole matrix for the pristine (6,5) single-walled carbon nanotube (SWCNT). The colorbar showcases the magnitude of the dipole matrix element. (b) Polaritonic energy as a function of the coupling strength A_0, where the cavity is in resonance with the bright E_{11} matter excitation ($\omega_c = 2.0$ eV). The colorbar indicates the percent of photonic character. (c-f) Excitonic absorption spectra plotted as a function of the transition energy and coupling strength A_0. The Lorentzian energy-broadening parameter is $\sigma = 0.1$ eV. The cavity frequency is taken to be (c) $\omega_c = 1.0$ eV (half-resonance), (c) $\omega_c = 1.5$ eV, (d,e) $\omega_c = 2.0$ eV (resonant with bright molecular transition, E_{11}), and (f) $\omega_c = 2.5$ eV. (Above) The polaritonic transition density at $A_0 = 0.0$ a.u. is shown above the spectra for the ground-to-bright E_{11} transition.

E_{11} state can be manipulated by tuning the cavity energy and coupling strength by either (d) blue-shifting or (f) red-shifting the bright state. In the ladder, the polaritonic system should be extremely emissive in the infrared telecommunications wavelengths. With low numbers of effective photons, this system could then operate as a source of single photons *without the need for covalent functionalization*. Until now, chemical functionalization was the only method to brighten the emission of these materials.[62,65]

In this letter, using time-dependent density functional theory (TD-DFT), we have studied *ab initio*, molecular exciton-polaritons, exploring various ways to analyze excited polaritonic states drawing from well-known excited state analysis methods from the electronic structure community. The community relies on simple methods to compute properties of excited states for high-throughput quantum chemistry, and with these tools, one is able to explore the physics and/or chemistry of any polaritonic system from first principles by focusing first on the complicated and computationally expensive molecular system, followed by the inclusion of the photonic degrees of freedom which can then be exactly diagonalized accounting for the exact electron-photon correlation up to the truncation of the basis size. This is in stark contrast to many recent works focusing on the development of electronic-photonic structure methods.[31,40,41,43,70,71]

There is strong merit to formulating such an approach as it allows a variational solution to the mixed electron-photon problem – meaning that the electronic and photonic bases are optimized to give the correct eigenstates of the QED Hamiltonian given only a few original adiabtic-Fock states as a starting point. However, there are two main issues at the present time: (I) These electronic-photonic structure methods are not widely available/tested in commercially available software. (II) These methods require treating the electronic and photonic DOFs on the same footing even though the photonic DOFs are much simpler than their electronic counterparts.

For example, in the coupled cluster approach,[42,43] the number of Fock states (*i.e.*, coupled cluster excitation operators) and interaction terms used dramatically increases the computational cost such that only two Fock states have

been utilized in recent works,[37,42] where some benchmarking has been done in model systems,[43] effectively limiting calculations to a specific high-cavity-energy regime with minimal relevant electronically excited states. In other methods, such as density functional theory, some implementations are limited to treating the electronic and photonic DOFs using the same exchange-correlation functional,[32] which shows performance similar to that of the Hartree-Fock method.[37,50] In this way, one sacrifices some part of the problem in order to treat the two parts of the system on the same footing. These current limitations can be alleviated by first solving the more complex molecular subsystem on its own before diagonalizing the full, electron-photon system giving, in principle, the exact electron-photon correlation.

Theoretical Details

In order to examine the excited state properties of the polaritonic systems, the computation of the individual properties of the isolated electronic and photonic systems must be first computed and then mixed through linear combinations by Eq. 6 to acquire the polaritonic properties. We will derive one example for clarity to outline the general procedure, but this can be simplified by using commercial electronic structure packages to obtain the final results for the bare electronic quantities. The one-particle transition density operator[31,51,72,73] between the α^{th} and β^{th} molecular states $\hat{\xi}^{\text{M}}_{\alpha\beta}$ is defined as

$$\begin{aligned}\hat{\xi}^{\text{M}}_{\beta\alpha} &= |\psi_\alpha\rangle\langle\psi_\beta| = \int d\mathbf{r}d\mathbf{r}'\psi_\alpha(\mathbf{r})\psi^*_\beta(\mathbf{r}')|\mathbf{r}\rangle\langle\mathbf{r}'| \quad (7)\\ &\equiv \int d\mathbf{r}d\mathbf{r}'\xi^{\text{M}}_{\beta\alpha}(\mathbf{r},\mathbf{r}')|\mathbf{r}\rangle\langle\mathbf{r}'|,\end{aligned}$$

where $\xi^{\text{M}}_{\beta\alpha}(\mathbf{r},\mathbf{r}') = \psi_\alpha(\mathbf{r})\psi^*_\beta(\mathbf{r}')$, $\psi_\alpha(\mathbf{r}) = \langle\mathbf{r}|\psi_\alpha\rangle$, and $\mathbf{r} = \{\mathbf{r}_1, \cdots, \mathbf{r}_{N_\text{e}}\}$, where N_e is the number of electrons. One can perform an integration over all but one of the electronic degrees of freedom (for both the primed and unprimed coordinates) and arrive at the molecular one-particle transition density matrix $\xi^{\text{M}}_{\beta\alpha}(\mathbf{r}_\text{e},\mathbf{r}_\text{h})$, defined as,

$$\xi^{\text{M}}_{\beta\alpha}(\mathbf{r}_\text{e},\mathbf{r}_\text{h}) = \int\prod_{i=2}^{N_\text{e}} \mathbf{dr}_i\mathbf{dr}'_i\langle\mathbf{r}_1\cdots\mathbf{r}_{N_\text{e}}|\hat{\xi}^{\text{M}}_{\beta\alpha}|\mathbf{r}'_1\cdots\mathbf{r}'_{N_\text{e}}\rangle, \quad (8)$$

where we have replaced $\mathbf{r}_1$ with $\mathbf{r}_\text{e}$ and $\mathbf{r}'_1$ with $\mathbf{r}_\text{h}$ on the left-hand side, which helps to signify that one may interpret the two coordinates as the electron and hole position in real space. One can also define the real-space projected transition density for the molecule,

$$\xi^{\text{M}}_{\beta\alpha}(\mathbf{r}_\text{e}) = \int\prod_{i=2}^{N_\text{e}} \mathbf{dr}_i\langle\mathbf{r}_1\cdots\mathbf{r}_{N_\text{e}}|\hat{\xi}^{\text{M}}_{\beta\alpha}|\mathbf{r}_1\cdots\mathbf{r}_{N_\text{e}}\rangle, \quad (9)$$

which is just the diagonal matrix elements of $\xi^{\text{M}}_{\beta\alpha}(\mathbf{r}_\text{e},\mathbf{r}_\text{h})$ in Eq. 8. Both $\xi^{\text{M}}_{\beta\alpha}(\mathbf{r}_\text{e},\mathbf{r}_\text{h})$ is readily available from most excited state electronic structure methods, such as CIS, TD-DFT, and EOM-CC.

The interpretation of the above transition density matrix $\xi^{\text{M}}_{\beta\alpha}(\mathbf{r}_\text{e},\mathbf{r}_\text{h})$ (in the real-space basis) is well-defined.[51] The off-diagonal elements give indication of the spatial coherence between the electron and hole coordinates, indicating the probability of finding an extra electron at $\mathbf{r}_\text{e}$ and a hole at $\mathbf{r}_\text{h}$ upon transition from adiabtic state ψ_α to ψ_β. The diagonal elements of this matrix can be thought of as the net charge induced at $\mathbf{r}$ upon the electronic transition. This quantity is zero when the electron and hole do no occupy the same $\mathbf{r}$ and can thus be thought of as an electron-hole overlap density.

The transition density operator for the ground to j_{th} state in the polaritonic system $\hat{\rho}_{0j}$ can be written as

$$\hat{\rho}_{0j} = |\Phi_j\rangle\langle\Phi_0| = \sum_{\alpha n}\sum_{\beta m} C^j_{\alpha n}(C^0_{\beta,m})^*|\psi_\alpha, n\rangle\langle\psi_\beta, m|, \quad (10)$$

where each polaritonic state has been expanded in the basis of molecular and photonic states (see Eq. 5). We are interested in examining the changes of the electronic part of the system as a result of hybridization, so we first trace out the photonic degrees of freedom and define the following molecular-projected transition density operator

$$\hat{\rho}^{\text{M}}_{0j} = \text{Tr}_\text{Ph}[\hat{\rho}_{0j}] = \sum_{\alpha\beta n} C^j_{\alpha n}(C^0_{\beta n})^*|\psi_\alpha\rangle\langle\psi_\beta|, \quad (11)$$

where we have explicitly used the orthonormality relation of the Fock states $\langle n|m\rangle = \delta_{nm}$. This expression implies that the $\hat{\rho}^{\text{M}}_{0j}$ mixes all molecular transition densities according to the expansion coefficients of the polaritonic states. One can perform an integration over all but one of the electronic DOFs, arriving at the matter-projected one-particle transition density matrix $\rho^{\text{M}}_{0j}(\mathbf{r}_\text{e},\mathbf{r}_\text{h})$ as fol-

lows,

$$\rho^{\mathrm{M}}_{0j}(\mathbf{r}_{\mathrm{e}},\mathbf{r}_{\mathrm{h}}) = \int \prod_{i=2}^{N_{\mathrm{e}}} \mathbf{dr}_i \mathbf{dr}'_i \langle \mathbf{r}_1 \cdots \mathbf{r}_{N_{\mathrm{e}}} | \hat{\rho}^{\mathrm{M}}_{0j} | \mathbf{r}'_1 \cdots \mathbf{r}'_{N_{\mathrm{e}}} \rangle$$
$$= \sum_{\alpha\beta n} C^{j}_{\alpha n} (C^{0}_{\beta n})^{*} \cdot \xi^{\mathrm{M}}_{\beta\alpha}(\mathbf{r}_{\mathrm{e}},\mathbf{r}_{\mathrm{h}}), \tag{12}$$

where $\xi^{\mathrm{M}}_{\beta\alpha}(\mathbf{r}_{\mathrm{e}},\mathbf{r}_{\mathrm{h}})$ is the bare molecular single-particle transition density (Eq. 8). The diagonal elements of $\rho^{\mathrm{M}}_{0j}(\mathbf{r}_{\mathrm{e}},\mathbf{r}_{\mathrm{h}})$ comprise the real-space projected transition density of the polariton system,

$$\rho^{\mathrm{M}}_{0j}(\mathbf{r}) = \sum_{\alpha\beta n} C^{0}_{\alpha n} (C^{j}_{\beta n})^{*} \cdot \xi^{\mathrm{M}}_{\beta\alpha}(\mathbf{r}), \tag{13}$$

where $\xi^{\mathrm{M}}_{\beta\alpha}(\mathbf{r}) \equiv \rho^{\mathrm{M}}_{0j}(\mathbf{r},\mathbf{r}) = \psi_{\alpha}(\mathbf{r})\psi^{*}_{\beta}(\mathbf{r})$. Recall that we have explicitly removed the photonic transition density from appearing, but, in principle, could also appear to give a more general expression. The generalization of Eq. 13 to include all possible one-particle matter, photonic, and mixed matter-photonic observables is shown in Eq. 6.

Natural transition orbital (NTO)[72–74] analysis is another, maybe even more common, method to understand the electron and hole distributions in real space, which can be readily evaluated by electronic structure packages through diagonalization (or rather singular value decomposition, in general) of the transition density matrix, $\xi^{\mathrm{M}}_{\beta\alpha}(\mathbf{r}_{\mathrm{e}},\mathbf{r}_{\mathrm{h}})$ (see Eq. 8). The dominant singular values $\{s_d\}$ represent the largest contributions to the electron and hole distributions in real-space for a particular $\alpha\beta_{\mathrm{th}}$ electronic transition while retaining the phase information of the orbitals. The transition orbitals are referred to as the highest occupied transition orbital (HOTO) $(\zeta^{\mathrm{H}}_{d})^{\mathrm{M}}_{\alpha\beta}$ and lowest unoccupied transition orbital (LUTO) $(\zeta^{\mathrm{L}}_{d})^{\mathrm{M}}_{\alpha\beta}$. For the NTOs presented in Fig. 3c-e, the polaritonic NTOs $(\Xi^{\mathrm{H/L}}_{d})^{\mathrm{M}}_{\alpha\beta}$ for a given polaritonic transition were constructed by computing the electronic NTOs for all bare molecular transitions $(\zeta^{\mathrm{H/L}}_{d})^{\mathrm{M}}_{\alpha\beta}$ followed by inserting into Eq. 6 with $\hat{B}_{\mathrm{ph}} = \hat{\mathbb{1}}_{\mathrm{ph}}$, where $\hat{\mathbb{1}}_{\mathrm{ph}}$ is the identity matrix for the photonic DOFs. This will give a similar result as that of Eq.13 where the photonic DOFs have been traced out, and the examination of the cavity-induced effects on the local electronic structure can be examined. The inclusion of such an analysis of the photonic DOFs are not required due to the simplicity of the single quantized cavity mode harmonic oscillator structure.

In Figs. 3 and 4, the excitonic absorption spectra was computed as,

$$A(E) = \sum_{j} f_{0j}\delta(E - \mathcal{E}_{0j}), \tag{14}$$

where $\mathcal{E}_{0j}$ is the transition energy between the ground and j_{th} polaritonic states and f_{0j} is the oscillator strength between the ground and j_{th} polaritonic state computed as,

$$f_{0j} = \frac{2}{3}\mathcal{E}_{0j}|\mu^{\mathrm{M}}_{0j}|^2. \tag{15}$$

Note that the delta-function in Eq. 14 is usually broadened with by a finite-width Gaussian or Lorentzian function to account for excitonic, photonic, and/or environmental relaxation/broadening processes present in realistic experimental conditions. Here, we chose to use a Lorentzian function where $\sigma = 0.1$ eV is the broadening parameter. In Eq. 15, μ^{M}_{0j} is the molecular part of the polaritonic dipole calculated from Eq. 6 with $\boldsymbol{\mu}^{\mathrm{M}}_{0j} = \hat{A}\hat{B} = \hat{\boldsymbol{\mu}} \otimes \hat{\mathbb{1}}_{\mathrm{ph}}$. The matrix elements of $\hat{\boldsymbol{\mu}}$ are computed according to Eq. 3.

In principle, another term should be added to account for the photonic part of the absorption/emission, which is proportional to $\hat{A}_{\mathrm{el}} \otimes \hat{B}^{\mathrm{ph}} \sim \hat{\mathbb{1}}_{\mathrm{el}} \otimes \hat{q}_{\mathrm{c}} \sim \hat{\mathbb{1}}_{\mathrm{el}} \otimes (\hat{a}^{\dagger} + \hat{a})$. However, the relative magnitude of the electronic and photonic contributions in experiment is extremely reliant on the experimental setup (*e.g.*, cavity loss, direction of the probe etc.). Other works have used different quantities to explore the cross-correlation of various observables for the spectroscopic analysis of molecular systems in cavities.[28] In experiment, usually the photonic contribution to the absorption and emission will dominate the intensity of the spectrum in Fabry–Pérot-type cavities.[75,76] However, for theoretical calculations, the excitonic absorption spectra (as well as other molecular properties), expressed here and in other works,[31,34,39,40] is better-suited to understand the effects of the cavity on the electronic sub-system and gives more direct insight into the *local* reactivity and *local* electronic reorganization in the molecule upon excitation of the polaritonic system. It is also important to recall that most of these reported results are in a single-mode cavity and, in principle, only represent the $\theta = 0$ special incident angle in a FP cavity.

Computational Details. All molecules were optimized with density functional theory (DFT) in the ground state electronic configuration, with-

out influence of the cavity. Formaldehyde, 35PPE, and H_2 utilized the B3LYP/6-311++G** while aminopropenal was calculated with ωB97XD/6-311++G**. The excited states were calculated with time-dependent DFT (TD-DFT) at the same level of theory. All DFT, TD-DFT, and natural transition orbital (NTOs)[74] calculations were performed using the Gaussian 16 software package.[77] The dipole matrix elements, real-space projected transition densities, and transition density matrices were computed using the Multiwfn v3.7 software package.[78]

For formaldehyde and aminopropenal, Eq. 4 was solved with 500 electronic states and 10 Fock states. For 35PPE, Eq. 4 was solved with 100 electronic states and 10 Fock states The H_2 molecule was solved in the basis of 3 electronic states and 5 Fock states.

The finite-size (6,5) SWCNT was constructed using the visual molecular dynamics (VMD) package[79] including 3 unit cells ($\sim$ 10 nm, 1092 atoms). The edges were properly capped with hydrogens according to previous works.[54,60,61,80–82] The SWCNT was optimized at the CAM-B3LYP/STO-3G level, followed by the calculation of the 20 lowest-energy vertical excitations at the same level of theory. This functional and basis has been shown to provide the correct excitonic localization and relative energies for these systems.[54–56,60,61,82] Eq. 4 was solved with 20 electronic states and 5 Fock states.

Acknowledgement This work was supported by the National Science Foundation "Center for Quantum Electrodynamics for Selective Transformations (QuEST)" under the Grant number CHE-2124398. Computing resources were provided by the Center for Integrated Research Computing (CIRC) at the University of Rochester. We thank Yu Zhang, Yihan Shao, and Jay Foley for helpful discussions.

Supporting Information Available

The Supporting Information contains additional dipole matrices for some molecules studied in this work as well as some additional plots regarding the tunability of the avoided crossing in formaldehyde.

References

(1) Nagarajan, K.; Thomas, A.; Ebbesen, T. W. Chemistry under Vibrational Strong Coupling. *J. Am. Chem. Soc.* **2021**, *143*, 16877–16889.

(2) Garcia-Vidal, F. J.; Ciuti, C.; Ebbesen, T. W. Manipulating matter by strong coupling to vacuum fields. *Science* **2021**, *373*, eabd0336.

(3) Hutchison, J. A.; Schwartz, T.; Genet, C.; Devaux, E.; Ebbesen, T. W. Modifying Chemical Landscapes by Coupling to Vacuum Fields. *Angewandte Chemie International Edition* **2012**, *51*, 1592–1596.

(4) Thomas, A.; Lethuillier-Karl, L.; Nagarajan, K.; Vergauwe, R. M. A.; George, J.; Chervy, T.; Shalabney, A.; Devaux, E.; Genet, C.; Moran, J.; Ebbesen, T. W. Tilting a ground-state reactivity landscape by vibrational strong coupling. *Science* **2019**, *363*, 615–619.

(5) Kowalewski, M.; Bennett, K.; Mukamel, S. Cavity Femtochemistry: Manipulating Nonadiabatic Dynamics at Avoided Crossings. *J. Phys. Chem. Lett.* **2016**, *7*, 2050–2054.

(6) Kowalewski, M.; Bennett, K.; Mukamel, S. Nonadiabatic dynamics of molecules in optical cavities. *J. Chem. Phys.* **2016**, *144*, 054309.

(7) Galego, J.; Garcia-Vidal, F. J.; Feist, J. Suppressing photochemical reactions with quantized light fields. *Nat Commun* **2016**, *7*, 13841.

(8) Herrera, F.; Spano, F. C. Cavity-Controlled Chemistry in Molecular Ensembles. *Phys. Rev. Lett.* **2016**, *116*, 238301.

(9) Ribeiro, R. F.; Martínez-Martínez, L. A.; Du, M.; Campos-Gonzalez-Angulo, J.; Yuen-Zhou, J. Polariton chemistry: controlling molecular dynamics with optical cavities. *Chem. Sci.* **2018**, *9*, 6325–6339.

(10) Feist, J.; Galego, J.; Garcia-Vidal, F. J. Polaritonic Chemistry with Organic Molecules. *ACS Photonics* **2018**, *5*, 205–216.

(11) Lacombe, L.; Hoffmann, N. M.; Maitra, N. T. Exact Potential Energy Surface for Molecules in Cavities. *Phys. Rev. Lett.* **2019**, *123*, 083201.

(12) Mandal, A.; Krauss, T. D.; Huo, P. Polariton-Mediated Electron Transfer via Cavity Quantum Electrodynamics. *J. Phys. Chem. B* **2020**, *124*, 6321–6340.

(13) Mandal, A.; Huo, P. Investigating New Reactivities Enabled by Polariton Photochemistry. *J. Phys. Chem. Lett.* **2019**, *10*, 5519–5529.

(14) Li, X.; Mandal, A.; Huo, P. Theory of Mode-Selective Chemistry through Polaritonic Vibrational Strong Coupling. *J. Phys. Chem. Lett.* **2021**, *12*, 6974–6982.

(15) Li, X.; Mandal, A.; Huo, P. Cavity frequency-dependent theory for vibrational polariton chemistry. *Nat Commun* **2021**, *12*, 1315.

(16) Martínez-Martínez, L. A.; Ribeiro, R. F.; Campos-González-Angulo, J.; Yuen-Zhou, J. Can Ultrastrong Coupling Change Ground-State Chemical Reactions? *ACS Photonics* **2018**, *5*, 167–176.

(17) Martínez-Martínez, L. A.; Du, M.; Ribeiro, R. F.; Kéna-Cohen, S.; Yuen-Zhou, J. Polariton-Assisted Singlet Fission in Acene Aggregates. *J. Phys. Chem. Lett.* **2018**, *9*, 1951–1957.

(18) Campos-Gonzalez-Angulo, J. A.; Ribeiro, R. F.; Yuen-Zhou, J. Resonant catalysis of thermally activated chemical reactions with vibrational polaritons. *Nat Commun* **2019**, *10*, 4685.

(19) Li, T. E.; Cui, B.; Subotnik, J. E.; Nitzan, A. Molecular Polaritonics: Chemical Dynamics Under Strong Light–Matter Coupling. *Annual Review of Physical Chemistry* **2022**, *73*, 43–71.

(20) Li, T. E.; Nitzan, A.; Subotnik, J. E. Polariton relaxation under vibrational strong coupling: Comparing cavity molecular dynamics simulations against Fermi's golden rule rate. *J. Chem. Phys.* **2022**, *156*, 134106.

(21) Li, T. E.; Nitzan, A.; Subotnik, J. E. Collective Vibrational Strong Coupling Effects on Molecular Vibrational Relaxation and Energy Transfer: Numerical Insights via Cavity Molecular Dynamics Simulations**. *Angewandte Chemie* **2021**, *133*, 15661–15668.

(22) Li, T. E.; Chen, H.-T.; Nitzan, A.; Subotnik, J. E. Quasiclassical modeling of cavity quantum electrodynamics. *Phys. Rev. A* **2020**, *101*, 033831.

(23) Fassioli, F.; Park, K. H.; Bard, S. E.; Scholes, G. D. Femtosecond Photophysics of Molecular Polaritons. *J. Phys. Chem. Lett.* **2021**, *12*, 11444–11459.

(24) Wei, Y.-C.; Lee, M.-W.; Chou, P.-T.; Scholes, G. D.; Schatz, G. C.; Hsu, L.-Y. Can Nanocavities Significantly Enhance Resonance Energy Transfer in a Single Donor–Acceptor Pair? *J. Phys. Chem. C* **2021**, *125*, 18119–18128.

(25) Lindoy, L. P.; Mandal, A.; Reichman, D. R. *Resonant Cavity Modification of Ground State Chemical Kinetics*; 2022.

(26) Xu, D.; Mandal, A.; Baxter, J. M.; Cheng, S.-W.; Lee, I.; Su, H.; Liu, S.; Reichman, D. R.; Delor, M. *Ultrafast imaging of coherent polariton propagation and interactions*; 2022.

(27) Ruggenthaler, M.; Flick, J.; Pellegrini, C.; Appel, H.; Tokatly, I. V.; Rubio, A. Quantum-electrodynamical density-functional theory: Bridging quantum optics and electronic-structure theory. *Phys. Rev. A* **2014**, *90*, 012508.

(28) Ruggenthaler, M.; Tancogne-Dejean, N.; Flick, J.; Appel, H.; Rubio, A. From a quantum-electrodynamical light–matter description to novel spectroscopies. *Nat Rev Chem* **2018**, *2*, 1–16.

(29) Flick, J.; Ruggenthaler, M.; Appel, H.; Rubio, A. Kohn–Sham approach to quantum electrodynamical density-functional theory: Exact time-dependent effective potentials in real space. *Proceedings of the National Academy of Sciences* **2015**, *112*, 15285–15290.

(30) Flick, J.; Appel, H.; Ruggenthaler, M.; Rubio, A. Cavity Born–Oppenheimer Approximation for Correlated Electron–Nuclear-Photon Systems. *J. Chem. Theory Comput.* **2017**, *13*, 1616–1625.

(31) Flick, J.; Narang, P. Ab initio polaritonic potential-energy surfaces for excited-state nanophotonics and polaritonic chemistry. *J. Chem. Phys.* **2020**, *153*, 094116.

(32) Pellegrini, C.; Flick, J.; Tokatly, I. V.; Appel, H.; Rubio, A. Optimized Effective Potential for Quantum Electrodynamical Time-Dependent Density Functional Theory. *Phys. Rev. Lett.* **2015**, *115*, 093001.

(33) Pavošević, F.; Flick, J. Polaritonic Unitary Coupled Cluster for Quantum Computations. *J. Phys. Chem. Lett.* **2021**, *12*, 9100–9107.

(34) Wang, D. S.; Yelin, S. F.; Flick, J. Defect Polaritons from First Principles. *ACS Nano* **2021**, *15*, 15142–15152.

(35) Juraschek, D. M.; Neuman, T.; Flick, J.; Narang, P. Cavity control of nonlinear phononics. *Phys. Rev. Research* **2021**, *3*, L032046.

(36) Rivera, N.; Flick, J.; Narang, P. Variational Theory of Nonrelativistic Quantum Electrodynamics. *Phys. Rev. Lett.* **2019**, *122*, 193603.

(37) Haugland, T. S.; Schäfer, C.; Ronca, E.; Rubio, A.; Koch, H. Intermolecular interactions in optical cavities: An ab initio QED study. *J. Chem. Phys.* **2021**, *154*, 094113.

(38) Flick, J.; Ruggenthaler, M.; Appel, H.; Rubio, A. Atoms and molecules in cavities, from weak to strong coupling in quantum-electrodynamics (QED) chemistry. *Proceedings of the National Academy of Sciences* **2017**, *114*, 3026–3034.

(39) Flick, J.; Welakuh, D. M.; Ruggenthaler, M.; Appel, H.; Rubio, A. Light–Matter Response in Nonrelativistic Quantum Electrodynamics. *ACS Photonics* **2019**, *6*, 2757–2778.

(40) Yang, J.; Ou, Q.; Pei, Z.; Wang, H.; Weng, B.; Shuai, Z.; Mullen, K.; Shao, Y. Quantum-electrodynamical time-dependent density functional theory within Gaussian atomic basis. *J. Chem. Phys.* **2021**, *155*, 064107.

(41) Vu, N.; McLeod, G. M.; Hanson, K.; DePrince, A. E. Enhanced Diastereocontrol via Strong Light–Matter Interactions in an Optical Cavity. *J. Phys. Chem. A* **2022**, acs.jpca.2c07134.

(42) Haugland, T. S.; Ronca, E.; Kjønstad, E. F.; Rubio, A.; Koch, H. Coupled Cluster Theory for Molecular Polaritons: Changing Ground and Excited States. *Phys. Rev. X* **2020**, *10*, 041043.

(43) Mordovina, U.; Bungey, C.; Appel, H.; Knowles, P. J.; Rubio, A.; Manby, F. R. Polaritonic coupled-cluster theory. *Phys. Rev. Research* **2020**, *2*, 023262.

(44) Wang, D. S.; Neuman, T.; Flick, J.; Narang, P. Light–matter interaction of a molecule in a dissipative cavity from first principles. *J. Chem. Phys.* **2021**, *154*, 104109.

(45) McTague, J.; Foley, J. J. Non-Hermitian cavity quantum electrodynamics–configuration interaction singles approach for polaritonic structure with ab initio molecular Hamiltonians. *J. Chem. Phys.* **2022**, *156*, 154103.

(46) Rokaj, V.; Welakuh, D. M.; Ruggenthaler, M.; Rubio, A. Light–matter interaction in the long-wavelength limit: no ground-state without dipole self-energy. *J. Phys. B: At. Mol. Opt. Phys.* **2018**, *51*, 034005.

(47) Riso, R. R.; Haugland, T. S.; Ronca, E.; Koch, H. Molecular orbital theory in cavity QED environments. *Nat Commun* **2022**, *13*, 1368.

(48) Riso, R. R.; Haugland, T. S.; Ronca, E.; Koch, H. On the characteristic features of ionization in QED environments. *J. Chem. Phys.* **2022**, *156*, 234103.

(49) Galego, J.; Garcia-Vidal, F. J.; Feist, J. Cavity-Induced Modifications of Molecular Structure in the Strong-Coupling Regime. *Phys. Rev. X* **2015**, *5*, 041022.

(50) Pavošević, F.; Hammes-Schiffer, S.; Rubio, A.; Flick, J. Cavity-Modulated Proton Transfer Reactions. *J. Am. Chem. Soc.* **2022**,

(51) Tretiak, S.; Mukamel, S. Density Matrix Analysis and Simulation of Electronic Excitations in Conjugated and Aggregated Molecules. *Chem. Rev.* **2002**, *102*, 3171–3212.

(52) Lüttgens, J. M.; Berger, F. J.; Zaumseil, J. Population of Exciton–Polaritons via Luminescent sp3 Defects in Single-Walled Carbon Nanotubes. *ACS Photonics* **2021**, *8*, 182–193.

(53) Möhl, C.; Graf, A.; Berger, F. J.; Lüttgens, J.; Zakharko, Y.; Lumsargis, V.; Gather, M. C.; Zaumseil, J. Trion-Polariton Formation in Single-Walled Carbon Nanotube Microcavities. *ACS Photonics* **2018**, *5*, 2074–2080.

(54) Gifford, B. J.; Saha, A.; Weight, B. M.; He, X.; Ao, G.; Zheng, M.; Htoon, H.; Kilina, S.; Doorn, S. K.; Tretiak, S. Mod(n-m,3) Dependence of Defect-State Emission Bands in Aryl-Functionalized Carbon Nanotubes. *Nano Lett.* **2019**, *19*, 8503–8509.

(55) Weight, B. M.; Sifain, A. E.; Gifford, B. J.; Kilin, D.; Kilina, S.; Tretiak, S. Coupling between Emissive Defects on Carbon Nanotubes: Modeling Insights. *J. Phys. Chem. Lett.* **2021**, *12*, 7846–7853.

(56) Weight, B. M.; Gifford, B. J.; Tretiak, S.; Kilina, S. Interplay between Electrostatic Properties of Molecular Adducts and Their Positions at Carbon Nanotubes. *J. Phys. Chem. C* **2021**, *125*, 4785–4793.

(57) He, X.; Gifford, B. J.; Hartmann, N. F.; Ihly, R.; Ma, X.; Kilina, S. V.; Luo, Y.; Shayan, K.; Strauf, S.; Blackburn, J. L.; Tretiak, S.; Doorn, S. K.; Htoon, H. Low-Temperature Single Carbon Nanotube Spectroscopy of sp ^{3}\$ Quantum Defects. *ACS Nano* **2017**, *11*, 10785–10796.

(58) He, X.; Velizhanin, K. A.; Bullard, G.; Bai, Y.; Olivier, J.-H.; Hartmann, N. F.; Gifford, B. J.; Kilina, S.; Tretiak, S.; Htoon, H.; Therien, M. J.; Doorn, S. K. Solvent- and Wavelength-Dependent Photoluminescence Relaxation Dynamics of Carbon Nanotube sp3 Defect States. *ACS Nano* **2018**, *12*, 8060–8070.

(59) Kwon, H.; Furmanchuk, A.; Kim, M.; Meany, B.; Guo, Y.; Schatz, G. C.; Wang, Y. Molecularly Tunable Fluorescent Quantum Defects. *J. Am. Chem. Soc.* **2016**, *138*, 6878–6885.

(60) Gifford, B. J.; Kilina, S.; Htoon, H.; Doorn, S. K.; Tretiak, S. Exciton Localization and Optical Emission in Aryl-Functionalized Carbon Nanotubes. *J. Phys. Chem. C* **2018**, *122*, 1828–1838.

(61) Gifford, B. J.; He, X.; Kim, M.; Kwon, H.; Saha, A.; Sifain, A. E.; Wang, Y.; Htoon, H.; Kilina, S.; Doorn, S. K.; Tretiak, S. Optical Effects of Divalent Functionalization of Carbon Nanotubes. *Chem. Mater.* **2019**, *31*, 6950–6961.

(62) Gifford, B. J.; Kilina, S.; Htoon, H.; Doorn, S. K.; Tretiak, S. Controlling Defect-State Photophysics in Covalently Functionalized Single-Walled Carbon Nanotubes. *Acc. Chem. Res.* **2020**, *53*, 1791–1801.

(63) Berger, F. J.; de Sousa, J. A.; Zhao, S.; Zorn, N. F.; El Yumin, A. A.; Quintana García, A.; Settele, S.; Högele, A.; Crivillers, N.; Zaumseil, J. Interaction of Luminescent Defects in Carbon Nanotubes with Covalently Attached Stable Organic Radicals. *ACS Nano* **2021**,

(64) Settele, S.; Berger, F. J.; Lindenthal, S.; Zhao, S.; El Yumin, A. A.; Zorn, N. F.; Asyuda, A.; Zharnikov, M.; Högele, A.; Zaumseil, J. Synthetic control over the binding configuration of luminescent sp3-defects in single-walled carbon nanotubes. *Nat Commun* **2021**, *12*, 2119.

(65) Zaumseil, J. Luminescent Defects in Single-Walled Carbon Nanotubes for Applications. *Advanced Optical Materials* **2022**, *10*, 2101576.

(66) Jeantet, A.; Chassagneux, Y.; Raynaud, C.; Roussignol, P.; Lauret, J. S.; Besga, B.; Estève, J.; Reichel, J.; Voisin, C. Widely Tunable Single-Photon Source from a Carbon Nanotube in the Purcell Regime. *Phys. Rev. Lett.* **2016**, *116*, 247402.

(67) Endo, T.; Ishi-Hayase, J.; Maki, H. Photon antibunching in single-walled carbon nanotubes at telecommunication wavelengths and room temperature. *Appl. Phys. Lett.* **2015**, *106*, 113106.

(68) Nutz, M.; Zhang, J.; Kim, M.; Kwon, H.; Wu, X.; Wang, Y.; Högele, A. Photon Correlation Spectroscopy of Luminescent Quantum Defects in Carbon Nanotubes. *Nano Lett.* **2019**, *19*, 7078–7084.

(69) Zheng, Y.; Han, Y.; Weight, B. M.; Lin, Z.; Gifford, B. J.; Zheng, M.; Kilin, D.; Kilina, S.; Doorn, S. K.; Htoon, H.; Tretiak, S. Photochemical spin-state control of binding configuration for tailoring organic color center emission in carbon nanotubes. *Nat Commun* **2022**, *13*, 4439.

(70) Liebenthal, M. D.; Vu, N.; DePrince, A. E. Equation-of-motion cavity quantum electrodynamics coupled-cluster theory for electron attachment. *J. Chem. Phys.* **2022**, *156*, 054105.

(71) DePrince, A. E. Cavity-modulated ionization potentials and electron affinities from quantum electrodynamics coupled-cluster theory. *J. Chem. Phys.* **2021**, *154*, 094112.

(72) Plasser, F.; Bäppler, S. A.; Wormit, M.; Dreuw, A. New tools for the systematic analysis and visualization of electronic excitations. II. Applications. *J. Chem. Phys.* **2014**, *141*, 024107.

(73) Plasser, F.; Wormit, M.; Dreuw, A. New tools for the systematic analysis and visualization of electronic excitations. I. Formalism. *J. Chem. Phys.* **2014**, *141*, 024106.

(74) Martin, R. L. Natural transition orbitals. *J. Chem. Phys.* **2003**, *118*, 4775–4777.

(75) Engelhardt, G.; Cao, J. Unusual dynamical properties of disordered polaritons in microcavities. *Phys. Rev. B* **2022**, *105*, 064205.

(76) Herrera, F.; Spano, F. C. Absorption and photoluminescence in organic cavity QED. *Phys. Rev. A* **2017**, *95*, 053867.

(77) Frisch, M. J. et al. Gaussian 16 Rev. C.01. 2016.

(78) Lu, T.; Chen, F. Multiwfn: A multifunctional wavefunction analyzer. *J. Comput. Chem.* **2012**, *33*, 580–592.

(79) Humphrey, W.; Dalke, A.; Schulten, K. VMD: Visual molecular dynamics. *J. Mol. Graph* **1996**, *14*, 33–38.

(80) Kilina, S.; Tretiak, S. Excitonic and Vibrational Properties of Single-Walled Semiconducting Carbon Nanotubes. *Adv. Funct. Mat.* **2007**, *17*, 3405–3420.

(81) Sharma, A.; Gifford, B. J.; Kilina, S. Tip Functionalization of Finite Single-Walled Carbon Nanotubes and Its Impact on the Ground and Excited State Electronic Structure. *J. Phys. Chem. C* **2017**, *121*, 8601–8612.

(82) Gifford, B. J.; Sifain, A. E.; Htoon, H.; Doorn, S. K.; Kilina, S.; Tretiak, S. Correction Scheme for Comparison of Computed and Experimental Optical Transition Energies in Functionalized Single-Walled Carbon Nanotubes. *J. Phys. Chem. Lett.* **2018**, *9*, 2460–2468.